Summary on Rayleigh and Rotational Raman Scattering for the ISSI Team of the NDACC Lidar Working Group

Thomas Trickl,

Karlsruher Institut für Technologie, IMK-IFU, Kreuzeckbahnstr. 19, 82467 Garmisch-Partenkirchen, Germany, thomas@trickl.de

December 14, 2013

Revised: June 5, 2023

1. Introduction

For fully quantitative retrievals of aerosol optical coefficients and temperature from lidar measurements a lot of details must be taken into consideration that cannot be neglected. This particularly obvious for temperature retrievals where a target uncertainty of (e.g.) 1 K means a relative uncertainty of the order of 0.3 %. In this chapter some of the most important issues are summarized.

There is a host of literature on the scattering of radiation in the atmosphere, with, in part, conflicting definitions and approaches. Most approaches are based on classical theory, but there are also mixed treatments where the detailed spectral structure of the scattered light due to Raman scattering are given by quantum theory and the overall budget by the classical equations. A good overview of the mixed method was given by She [1], but the validity of the mixed approach is not discussed. Another review was more recently published by Eberhard [2]. Pure quantum approaches (e.g., [3-5]) concentrate on side scattering which is the configuration for laboratory experiments. An exception is the theory by Sharma [6], but these expressions seem to be restricted to single lines of the Raman Q branch.

Scattering of radiation by the air components N_2 (78.084 %), O_2 (20.946 %), Ar (0. 934 %) and CO_2 (0.0397 %), values from http://en.wikipedia.org/wiki/Atmosphere_of_Earth) leads to slight depolarization of the outgoing radiation attributed to rotational Raman scattering from the molecular components. Unfortunately, the use of "depolarized" in the literature is frequently misleading, which may have consequences on the detailed results and, therefore, suggested a careful re-examination of the theoretical background. The mixed classical and quantum-mechanical procedure is used here since quantitative measurements of the classical quantities exist and can be used to calibrate the spectra. This seems to be justified since the sums of the Raman line strengths get close to the corresponding classical expressions (see further below).

Two components determine the scattered intensity, the electronic portion determined by the refractive index of air and the rotational Raman scattering intensity (O, Q and S branches). Young named the sum of Q branch and the non-Raman part Cabannes line (for more information on the detailed Rayleigh-Brillouin line shape see Ref. 7) and the overall emission including also the rotational satellites Rayleigh scattering [8]. This convention is adopted here.

For lidar systems not implying any spectral filtering in the receiver also the ro-vibrational Raman scattering must be taken into consideration. This effect, however, is of the order of 0.1 % of the overall backscatter signal [9] and, thus, even smaller than the uncertainty level specified above for the temperature measurements.

2. Total Extinction Cross Section

The total cross section of Rayleigh scattering can be calculated with high accuracy from

$$\sigma_R = \frac{32\pi^3}{3\lambda^4 N^2}(n-1)^2 F_K, \quad [10] \tag{1}$$

with the refractive index n, the air number density N and the King correction factor F_K which departs from 1 in the case of anisotropic scattering (Raman scattering). The refractive index of air can be computed with a relative uncertainty of 10^{-7} from the theory of Owens [11], revised by Ciddor [12] for reaching an uncertainty of the order of 10^{-8}. These two approaches also include water vapour and corrections for non-ideal-gas behaviour of air. The algorithm of Ref. 12 was implemented for the lidar systems at Garmisch-Partenkirchen in 1991 [13], and never upgraded with reference 12 because of sufficient accuracy and a clearer description. There is one deficiency in this approach. Both Owens and Ciddor use the Lorentz-Lorentz formalism for calculating the refractive index, i.e.,

$$\frac{n^2-1}{n^2+2} = \sum_{i=1}^{m} \frac{n_i^2-1}{n_i^2+2} \frac{\rho_i}{\rho_{o,i}} \ , \tag{2}$$

for m-component air, ρ_i and $\rho_{o,i}$ being the partial densities of the i-th component and a reference partial density, respectively. For instance in Ref. 12 $\rho_{o,1}$ (dry, CO_2-free air) is given for 1013.25 mbar and 288.16 K. Equation 2 is more adequate in dense media [14]. Since the refractive indices derived from Eq. 2 scale approximately as the true densities, $n - 1$ after a transfer into Eq. 1 does not. Although this discrepancy as a function of the density is less than 10^{-3} of the value we for some time preferred to calculate σ_R for standard conditions [13]. Later it turned out that this is not necessary if one adopts the Lorentz-Lorentz formalism also for calculating the polarizability in the case of Rayleigh scattering. Equation 1 is then rewritten as

$$\sigma_R = \frac{24\pi^3}{\lambda^4 N^2} \frac{(n^2-1)^2}{(n^2+2)^2} F_K \ . \tag{3}$$

The result of this expression and simplifying substitutions is shown in Fig. 1:

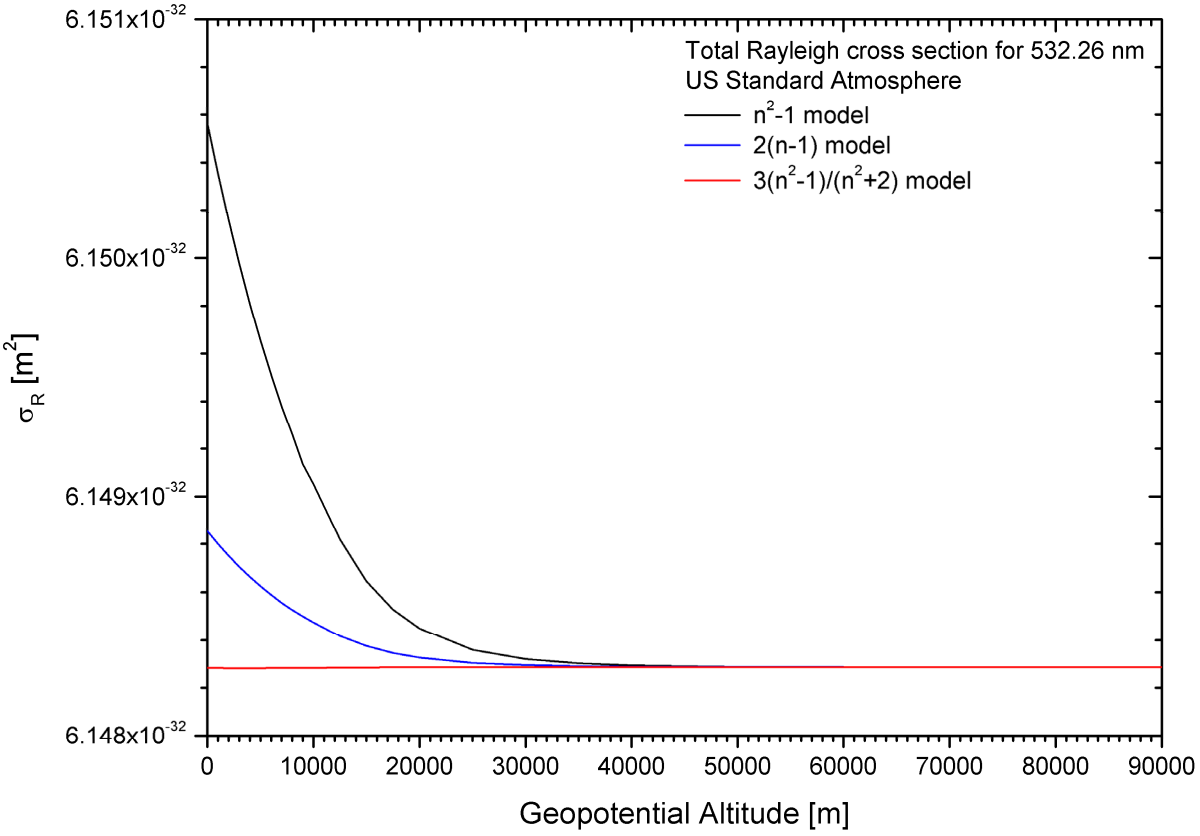

Fig. 1: Total Rayleigh cross section for the vacuum wavelength 532.26 nm, calculated for air densities from interpolated pressures and temperatures of the 1976 US Standard Atmosphere [15]; the refractive index n is calculated

from the theory of Owens [11]. Three models for σ_R are compared: a model in which $n-1$ in Eq. 1 is replaced by $0.5*(n^2-1)$ (black, not discussed here), as well as the models of Eq. 1 (blue) and Eq. 3 (red).

As expected the variation of the cross section as a function of the air density is rather low for for Eq. 3 (a few times 10^{-7}), the maximum relative deviation for Eq. 1 being 9.3×10^{-5} for 1013.25 mbar and 288.15 K (sea level). Similar deviations are obtained for other wavelengths, with 1.08×10^{-4} at 200 nm being the maximum relative deviation for wavelengths ≤ 200 nm. Figure 1 clearly shows that the calculation of σ_R for Eq. 1 for standard conditions, as done by us before, yields the worst result if Eq. 1 is taken.

3. Laboratory Studies

For understanding the meaning of the various quantities it is necessary to understand both the measurement procedures and the theoretical treatment. Typically, there are three types of experiments yielding information on the Rayleigh extinction cross section, interferometric, depolarization and extinction measurements.

The refractive index has been accurately determined by interferometric techniques, i.e., by measuring the wavelength change due to filling a specific gas or air into a vacuum chamber (e.g, [16,17]). Not only the refractivity $n - 1$, but also the density dependence of the Lorentz-Lorentz ratio (Eq. 2) is derived by comparing the result for two different interference orders and two different densities [16]. An expression for the compressibility of the sample gas is also included in the mathematical treatment. It is reasonable to assume that the results of this interferometric procedure are not influenced by the shifted lines of the O- and S-branch rotational Raman spectrum. A contribution of the Q branch to the refractive index is excluded by She [1] and by Miles at el. [18] without clear explanation. This would mean that the Raman Q-branch is also included in F_K, and not in the other terms of Eqs. 1 or 3. In absence of contradicting papers we adopt this view.

The King factors of the most important atmospheric constituents and air have mostly been determined in depolarization measurements. The uncertainty in the King factors, also implying the Raman Q-branch issue, currently determines the overall uncertainty of the Rayleigh extinction coefficients, unless there is some problem with the definitions. There are differences between the classical and quantum-mechanical theories.

The treatment here follows Bates who used F_K values for the individual components of air and theoretical expressions for determining the overall King factor and its wavelength dependence [19]. The uncertainty of this procedure is specified as 1 % [19]. Bates does not give the details of his procedure that is based on experiments of different accuracy, based either on classical or quantum-mechanical approaches, and wavelength dependences introduced from ab-initio molecular calculations.

The King factor of air was synthesized by Bates by applying

$$F_K = \sum_{i=1}^{m} f_i F_K(i), \tag{4}$$

for air with the $m = 4$ components N_2, O_2, Ar, and CO_2 and their fractions f_i. Equation 5 is a direct consequence of

$$\sigma_R = \sum_{i=1}^{m} f_i \sigma_R(i),$$

if one assumes that $N_i = f_i N$ and that the factors containing the refractive index in Eqs. 1 and 3 are proportional to N^2 (or N_i^2 for the individual components).

A least-squares fit to the $F_K - 1$ values of Bates (200 nm ≤ λ ≤ 1000 nm), using the expression

$$F_K - 1 = \sum_{i=0}^{2} p_i \lambda^{-2i} \ , \tag{5}$$

λ in nm, yields the fit parameters (in brackets: relative standard deviations):

$p_0 = 4.69541179\times10^{-2}$ (3.49×10^{-3}),
$p_1 = 3.25031532\times10^{+2}$ (1.06×10^{-1}),
$p_2 = 3.86228507\times10^{+7}$ (3.63×10^{-2}).

The fitting procedure yields an average a-posteriori standard deviation of the approximation to the Bates data of 0.000402, corresponding to an average approximation of the $F_K - 1$ data within 0.51 % and 0.85 % between 200 nm and 1000 nm, respectively.

Finally, the listings of the overall Rayleigh extinction cross sections σ_R by Bates [19] exhibit a positive offset of just 0.066 % (400 nm) to about 0.25 % (200 and 1000 nm) with respect to an approach based on the refractive-index model in Ref. 10 and Eq. 4 and are, therefore, a useful set of data for most applications. The offset is presumably related to a difference the refractive index data used. The King factors of Bates were determined independently and do not correlate with deviations related to the refractive index (see below).

The 1-% level of uncertainty for σ_R for the most abundant atmospheric species, nitrogen, was confirmed in a more recent laboratory study, based on cavity ring-down spectroscopy, for Ar, N_2 and SF_6 by Naus and Ubachs [20] and Sneep and Ubachs [21] in a wavelength range between 470 nm and 650 nm. The data agree with the best model expression from the literature within typically 4%, a fit to these data even within 0.5 % and mostly less. A comparison of the same group in the deep ultraviolet between 197 nm and 270 nm was less successful [22]. The two values for N_2 specified by the authors as the best (for 198.48 nm and 251.72 nm) deviate from the σ_R values synthesized from equations from Ref. 19 by 0.18 % and 8.2 %, respectively. Here, it is important to mention that the refractive index model for nitrogen as specified by Bates [19] is applicable within an uncertainty of 0.2 % down to 156 nm, i.e., even below the lower limit (200 nm) of its range of validity (comparison with data from Ref. 23). This reflects the moderate wavelength dependence of that individual-component King factor.

The probably most accurate determination of the King factor is based on measurements of the depolarization ratio for nitrogen, oxygen and carbon dioxide by Bridge and Buckingham at the vacuum wavelength of 633.99 nm [3]. The values were determined from transverse scattering. From the expressions for F_K as a function of the depolarization factor in Ref. 1, propagation of the errors specified in Ref. 3, and the fractions f_i we obtain 1.04794±0.0039 for air. This value is almost perfectly reproduced by Eq. 5 (1.048006). Larger uncertainties must be considered for the ultraviolet spectral region where the wavelength dependence is more pronounced. Clearly, some improved laboratory measurements are desirable. There is a slight uncertainty in Ref. 3 about the "quantum correction" due to a potential mismatch of the formulae (Eqs. 25-27 in Ref. 3). However, this uncertainty is judged to be only important for the lightest molecules such as H_2 and D_2.

4. Backscatter Cross Sections

There is a caveat for Rayleigh backscattering. The backscatter differential cross sections are not obtained just by multiplying σ from Eqs. 1 or 3 by the backscatter-to-extinction ratio (3 sr^{-1})/8π as most commonly done for lidar applications.

Following She [1] the two polarization components of the differential scattering cross section for linearly polarized incident lights are

$$\frac{d\sigma_1}{d\Omega}(\pi) = \frac{\nu\ \pi^2}{\lambda_s^4 \nu_s} \frac{\gamma^2}{15} \ , \tag{6a}$$

$$\frac{d\sigma_2}{d\Omega}(\pi) = \frac{\nu\,\pi^2}{\lambda_s^4 \nu_s}(\alpha^2 + \frac{4\gamma^2}{45}), \tag{6b}$$

α and γ being the isotropic and anisotropic parts of the polarizability and the index s referring to "scattered". The ratio of the terms containing γ almost equals that of the quantum-mechanical branches (Sec. 5).

For unpolarized detection the total backward differential scattering cross section is then the sum of both components

$$\frac{d\sigma_R}{d\Omega}(\pi) = \frac{\nu\,\pi^2}{\lambda_s^4 \nu_s}\alpha^2(1 + \frac{7}{45}\frac{\gamma^2}{\alpha^2}). \tag{6c}$$

For polarization-sensitive detection one has to include the sensitivities for both orientations of the polarization. A full list of the classical expressions for different polarizations of light source or detection system is given (e.g.) by Kattawar et al. [23].

By integrating the full angle-dependent equations corresponding to Eqs. 6 [1] (or more complex [18]) over 4π one arrives at

$$\sigma_R = \frac{8\pi}{3}\frac{\nu\,\pi^2}{\lambda_s^4 \nu_s}\alpha^2(1 + \frac{2}{9}\frac{\gamma^2}{\alpha^2}) \tag{7}$$

and $$F_K = 1 + \frac{2}{9}\frac{\gamma^2}{\alpha^2}. \tag{8}$$

This form of F_K is found in all publications studied in this investigation. Equations 6 seem to be supported by the quantum-mechanical theory. The consequence of Eqs. 6 is that

$$\frac{8\pi}{3}\frac{\nu\,\pi^2}{\lambda_s^4 \nu_s}\alpha^2 = \frac{24\pi^3}{\lambda^4 N^2}\frac{(n^2-1)^2}{(n^2+2)^2},$$

if Eq. 3 is applied. The refractive index is related to the full polarizability of the bound electrons. It is not *a priori* obvious why the anisotropic component of the polarizability does not contribute to the values very accurately determined by interferometry. One explanation could be the random orientation of the molecules: The refractive-index measurements just determine the average properties. An experiment with oriented molecules would be interesting.

If one accepts the above setting, finally, a comparison of Eqs. 6c and 7 yields

$$F_K(\pi) = 1 + 0.7(F_K - 1). \tag{9}$$

For 532.24 nm [24] the error of setting $F_K(\pi) = F_K$ as frequently found in the lidar literature means a change in backscatter coefficient of just −1.39 %, for 354.827 nm −1.48 %. This deviation is small, but cannot be neglected in demanding applications. In the stratosphere, however, the role of the Rayleigh extinction coefficients strongly diminishes due to the low air density. In the UV the extinction is stronger due to the λ^{-4} wavelength dependence and must be calculated with care in the lower stratosphere, in particular for temperature retrievals.

5. Raman Scattering

The details of Raman scattering must be taken into consideration if the lidar return is spectrally filtered. Some properties are also required for the calibration of the Raman components.

The most important facts are listed in the following paragraphs:

(1) The rotational spectrum consists of three branches, named O, Q and S branch, corresponding to $\Delta J = -2, 0$, and $+2$, respectively.

(2) The spectrum of nitrogen, as a consequence of nuclear angular momentum I = 1, exhibits an intensity modulation (see 4.): Even J possess the weight 6 (F = 0 and F = 2, (2*0 + 1) + (2*2 + 1), odd J the weight 3 (F = 1, 2*1 + 1).

(3) For oxygen I = 0, which leads to exclusively odd J components.

(4) The relative population of a single J state is degeneracy factor d(F,J) times Boltzmann factor b(J) divided by the sum of all d(F,J)*b(J):

$d(F,J)=(2 F_1 + 1) (2 F_2 + 1) (2 J + 1)$,

$b(J) = \exp(-\Delta E(J)/(kT)$,

$\Delta E(J) = B J (J +1) - D [J (J + 1)]^2 + H [J (J + 1)]^3$.

The nitrogen data for the simulations underlying this chapter are taken from Refs. 24-25, the oxygen data are from Ref. 26 (see also Ref. 27).

(5) The line strengths are $S_J/(2J + 1)$, with the Placzek-Teller factors S_J [30,31], adopted from Ref. 32:

O branch: $S_J = 3 J (J - 1) / [2 (2 J - 1)]$ (10)

Q branch: $S_J = a_0 (2 J + 1) + J (J + 1) (2 J +1) / [(2 J - 1) (2 J + 3)]$ (11)

S branch: $S_J = 3 (J + 1) (J + 2) / [2 (2 J + 3)]$ (12)

The sum over all S_J is 2 J + 1. Placzek and Teller [30] state that $a_0 = 0$ (a_0 being proportional to the square of quantum number K) for molecules "in the ground state of the oscillation", in particular for Σ states, which applies for both nitrogen and oxygen.

(6) The sums over all line strengths of the O and the S branch are temperature-dependent. However, the sum of the O and S branch line strengths, as well as that of the Q branch line strengths, is almost temperature independent. For nitrogen one obtains for the normalized sum of line strengths:

T [K]	O branch	S branch	O plus S branch	Q branch
220	0.29659	0.44708	0.74367	0.25633
240	0.29992	0.44409	0.74400	0.25600
260	0.30286	0.44144	0.74429	0.25571
280	0.30548	0.43907	0.74455	0.25545
300	0.30784	0.43695	0.74479	0.25521

The sums in columns 4 and 5 are close to 0.75 and 0.25, respectively, the values of the classical theory. The sum of the values for all three branches is exactly 1, independent of temperature. As a result, by calculating the sums, the cross sections can to a good approximation be calibrated by replacing the factors for classical light scattering by average values for columns 4 and 5. Of course, also the filter transmission curves must be taken into account. The sums for oxygen are almost the same. However, this calculation was based on the same J model as for N_2, specified above (Items 4 and 5). The situation for O_2 is more complex due to the triplet splitting of the order of 0.05 cm^{-1} [6,28]. A simplified treatment analogous to that for nitrogen (applying the different sequence of line intensities (3)) yields only slightly different results:

T [K]	O branch	S branch	O plus S branch	Q branch
220	0.30473	0.43280	0.73753	0.26247
240	0.30787	0.43055	0.73842	0.26158
260	0.31064	0.42856	0.73919	0.26081
280	0.31310	0.42676	0.73985	0.26015
300	0.31530	0.42514	0.74044	0.25956

Here, the agreement of the sums with the classical fractions 0.75 and 0.25 is just slightly less good as in the case of N_2. For most applications the classical fractions of 0.25 (Q branch) and 0.75 (S plus O branch) are a good approximation because of the small size of the Raman contribution.

(7) For linearly polarized incident light the Raman lines are 75 % depolarized for both O and S branch. This looks confusing at a first glance since 75 % is also the total fraction of inelastic Raman scattering (see above). According to various publications (e.g., [18,33,34]) the Q branch lines are also 75 % depolarized. The Q_0 line does not exist for N_2 and O_2 (Eq. 11). This is not the case for the vibrational-rotational Raman scattering [35,36].

A 75 % depolarization is a general property of the rotational Raman lines for $^1\Sigma$ molecules [3]. If one includes the strong central component, the degree of polarization is just 1 % for, e.g., nitrogen [3].

(8) Quantitative measurements of the Q-branch depolarization ratios ($I_\perp/I_{|||}$) exist for ro-vibrational Raman scattering of hydrogen and deuterium [35,36]. They are substantially smaller than 0.25, particularly for the Q branch. The Q-branch depolarization ratio for H_2 is as low as 0.002 at J = 0, maximizes at J = 1 with 0.021 and gradually diminishes towards 0.0123 for higher J [36]. For the $v = 0 \rightarrow v = 0$ Q branch measurements are demanding because the individual J lines are degenerated and superimposed by the strong elastic contribution. Eloranta and Piironen derived a finite depolarization ratio of about 1 % from measurements with a high-spectral-resolution lidar [37]. This ratio is about three times the classical value and, thus, definitively not negligible, in agreement with a finite Q-branch depolarization. Cooper et al. indicate agreement with the expectations, but their study focusses on pressure effects and no quantitative number on the degree of depolarization is given [38]. The reason for the difference was not specified. It is reasonable to adopt the classical value of 75 %.

Calibration of the Raman spectrum

The calibration of the Raman spectrum is achieved by calculating the backward King factor (Eq. 9) based on the polynomial below Eq. 5. For the classical theory the Q branch contribution for unpolarized detection is derived from Eqs. 6c and 9 as

$$\frac{d\sigma_Q}{d\Omega}(\pi) = 0.25\frac{\nu\,\pi^2}{\lambda_s^4 \nu_s}\alpha^2\left[0.7(F_K - 1)\right] = 0.25\frac{\nu\,\pi^2}{\lambda_s^4 \nu_s}\alpha^2\left[\frac{7}{45}\frac{\gamma^2}{\alpha^2}\right] \tag{13}$$

For the sum of the S and O quantity 0.25 must be replaced by 0.75.

For polarized detection more detailed expressions are needed that can be derived from equations in Sec. 5. In the case of narrow-band detection the overlap of the spectral filter used with the S and O branch must be calculated. Approximations may suffice in the case of aerosol retrievals. However, for temperature retrievals with an uncertainty level of the order of 1 K or 0.3 % the overlap must be evaluated with particular care.

For a more quantitative approach the partial King factors for nitrogen and oxygen must be evaluated [19]:

$$F_K(N_2) = 1.034 + 317\ \lambda^{-2}, \quad (14)$$

$$F_K(O_2) = 1.096 + 1385\ \lambda^{-2} + 1.448\times10^{-8}\ \lambda^{-4}, \quad (15)$$

λ in nm. These expressions are used to calibrate the sums of the respective quantum expressions. Finally, the total F_K is calculated by using Eq. 5.

Other Sources of Uncertainty

The uncertainties of calculating the Rayleigh cross sections can be kept at the level of 1 % and less, if the vertical distribution of the factors determining the refractive index is sufficiently accurate.

At high pressures the air cannot be considered to be an ideal gas. Owens includes real-gas corrections in his refractive-index model [11]. In Fig. 2 the relative correction derived from Eq. 9 in Ref. 11 is displayed for a number of pressures and temperatures.

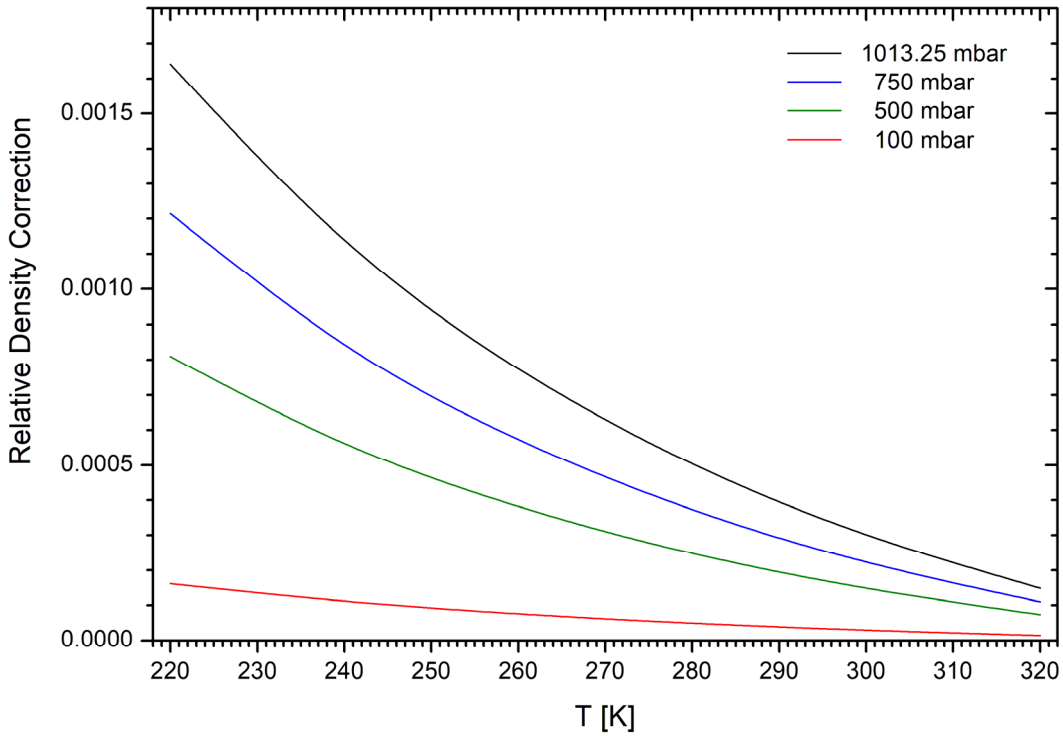

Fig. 2: Relative correction factors for the density of dry air free of CO_2 from Eq. 9 in Ref. 11

It is obvious that the correction factors are of the order of 1×10^{-3} and less under realistic atmospheric conditions. This is much lower than the relative uncertainties of the Rayleigh backscatter and extinction coefficients. Thus., real-gas corrections can be neglected.

A considerably higher uncertainty is caused by that of the radiosonde and model data used for calculating the Rayleigh backscatter coefficients. Radiosonde data from nearby routine sounding stations are normally available for 0:00 UTC and 12:00 UTC. The radiosonde models have been thoroughly compared in numerous field studies ([39] and references therein). There are discrete steps in the values between different generations. For the RS92 sonde from Vaisala there is an obvious temperature bias in the stratosphere, verified by lidar measurements at Hohenpeißenberg. This bias is likely to be due to wrong radiations of one or the other sonde types, during daytime mostly by that of the RS92 sonde. This bias can be as high as 1 K at altitudes corresponding to 10 mbar of atmospheric pressure. The error of the pressure values cannot be neglected. There is a contribution from wrong altitude determination that can amount to as much as –0.4 mbar at 10 mbar (about 30 km) for the RS80 sonde [39] which is by no means negligible. For the RS92 sonde the uncertainty is most likely within ±0.1 mbar (±1 % or better). The relative deviation diminishes towards lower altitudes for both sonde types. The new RS41 sonde should be similarly reliable.

For higher altitude model data derived from satellite measurements are used such as NCEP (National Centers for Environmental Prediction) data. These data are calculated for the positions of all NDACC stations up to about 55 km for 12 UTC. No information on the reliability of these data has been collected for this report. For the period starting in 2017 the aerosol measurements at Garmisch-Partenkirchen have gained in accuracy. No discrepancies were found in all these measurements with the profiles from Rayleigh simulations up to almost 50 km. In addition, a few temperature measurements up to the mesosphere have contributed to verifying the reliability of the NCEP data at a level of 1 % [40].

Alternatively, Raman signals could be used, but this requires long averaging times for sufficient quality in the stratosphere.

It is reasonable to assume that the relative uncertainty of the temperature data is lower than that of the pressure data. The pressure profile can then be obtained by integrating

$$\frac{d\ln \mathrm{P}}{d\mathrm{z}} = -\frac{\mathrm{M}\ \mathrm{g(z)}}{\mathrm{R_m T(z)}} \tag{17}$$

with the acceleration of gravity

$$g(z) = g(0)\left(\frac{\mathrm{r_0}}{\mathrm{r_0}+z}\right)^2 . \tag{18}$$

In Ref. 15 the values of the quantities in Eqs. 15 and 16 are given as M = 28.9644 kg/kmol (molar mass), R_m = 8314.32 N m /(kmol K) (universal gas constant), r_0 = 6356766 m (earth radius corresponding to sea level), and g(0) = 9.80665 m/s^2 [15]. Just the integration constant P(z_0) (ground value) must be introduced for calibration. It is important to note that no correction for real-gas behaviour is needed for Eq. 15 since the density was eliminated in its derivation [15].

Please, note that the sonde files contain the geopotential altitude

$$\mathrm{h_g} = \frac{\mathrm{r_0 z}}{\mathrm{r_0}+\mathrm{z}} \tag{19}$$

$$(\text{and } \mathrm{z} = \frac{\mathrm{r_0 h_g}}{\mathrm{r_0}-\mathrm{h_g}}) .$$

rather than z. A conversion must be made prior to integration. Using the geopotential altitude h_g instead of the real altitude z is not important at 10 km: h_g = 10000 m corresponds to z = 10016 m. But at h_g = 30000 m the positive deviation of z is already 142 m which is seven times the uncertainty specified for the RS92 sonde as estimated from the onboard GPS sensor. This results in a –2.1-% offset in pressure. Since the bias of the number density is dominated by that of the pressure it can be directly transferred to the Rayleigh backscatter coefficient. The error grows further at altitudes beyond 30 km.

Linear interpolations of pressure data from the sonde listing are much more accurate if made in logarithmic representation. For the temperature a linear scale is sufficient.

Examples are given in Figs. 2 and 3 where pressures calculated from radiosonde temperatures using Eq. 17 are compared with those listed for the same ascent (source: http://weather.uwyo.edu/upperair/ sounding.html). The pressure differences stay below ±1.0 mbar. The relative differences exhibit growing negative values, but this changes from ascent to ascent, which suggests no systematic behaviour. The relative deviations mostly stay below 0.5 %. For

comparison, the results for carrying out the same procedure for the US Standard Atmosphere [15] are given, multiplied by ten to make the very small differences visible. These differences of 0.006 % and less can be most likely ascribed to rounding-related errors in the tables of Ref. 15.

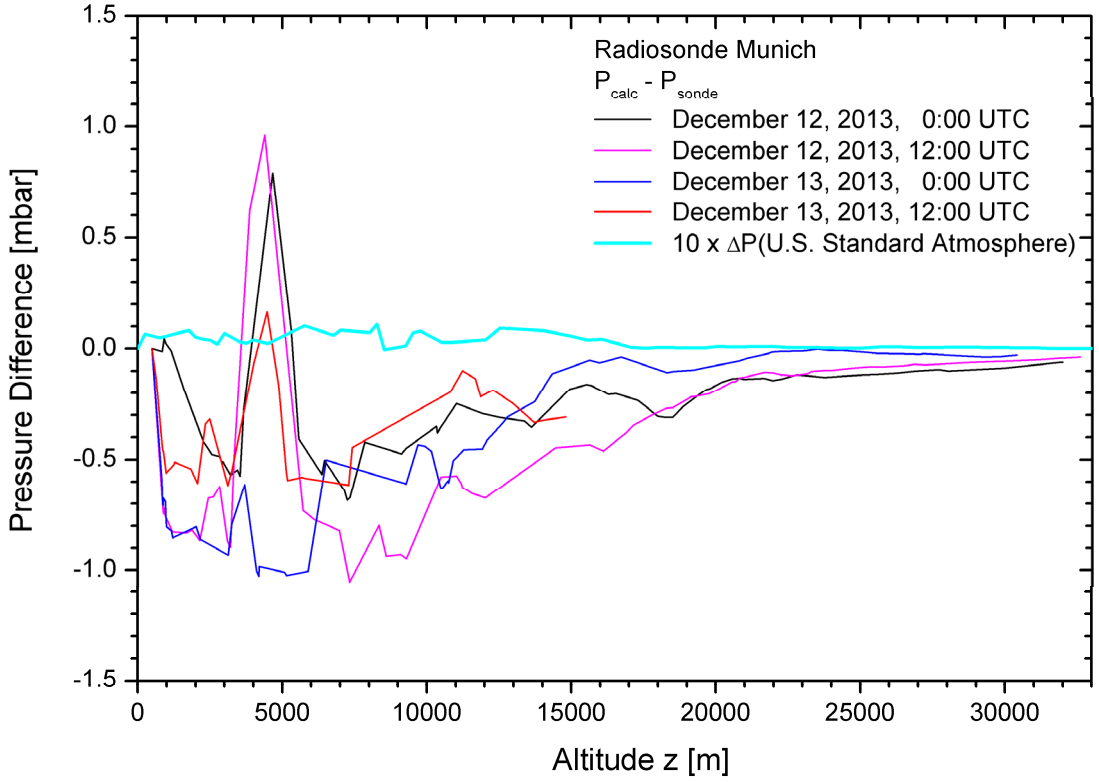

Fig. 3: Differences of the pressures calculated from radiosonde temperatures and the pressures listed for the same ascent. For comparison the results for Ref. 15 are given, multiplied by ten.

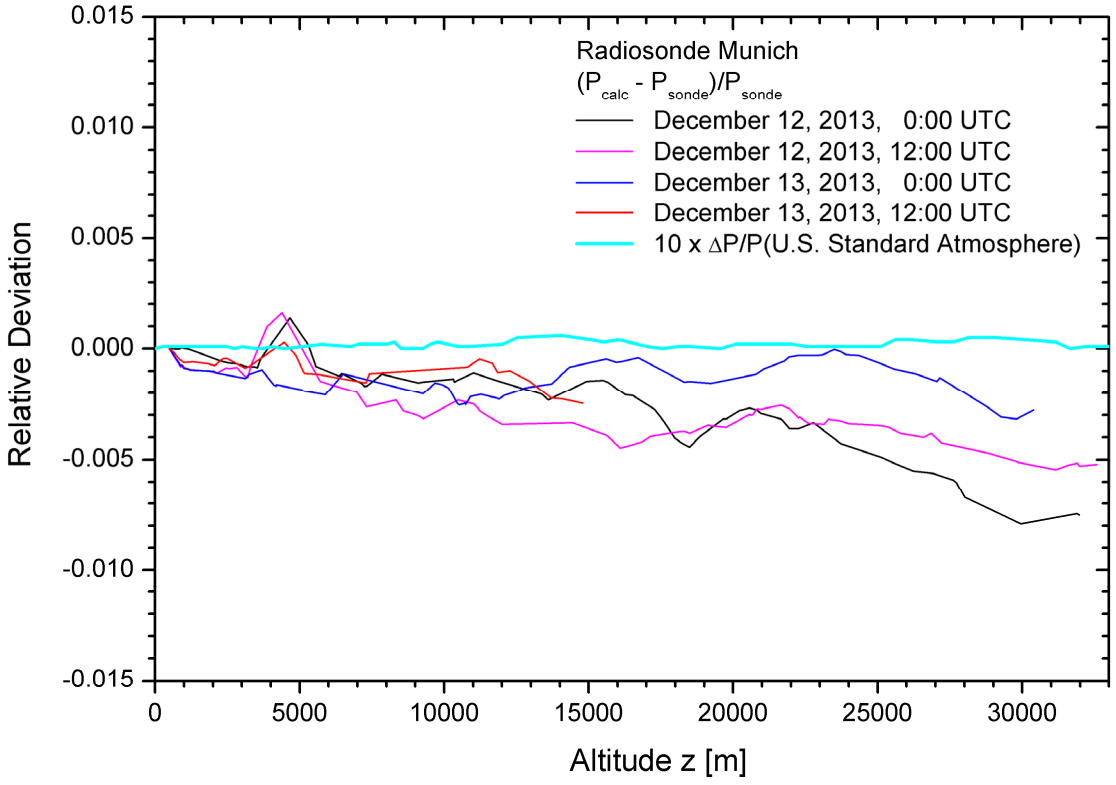

Fig. 4: Relative differences of pressures calculated from radiosonde temperatures and the pressures listed for the same ascent. For comparison the results for Ref. 15 are given, multiplied by ten in order to make visible the differences.

Above the maximum altitude reached by the weather balloons (30 km to 33 km) we have traditionally used NCEP (National Centers for Environmental Prediction) meteorological data daily calculated for 12 UTC for NDACC stations [41]. These data are listed for altitudes up to about 55 km and have been successfully validated by high-quality aerosol [42] and temperature [43] measurements. One example of a successful temperature comparison between a lidar measurement at Garmisch-Partenkirchen and the corresponding NCEP and radiosonde temperature profile is shown in Fig. 5. The temperatures agree within less than 2 %.

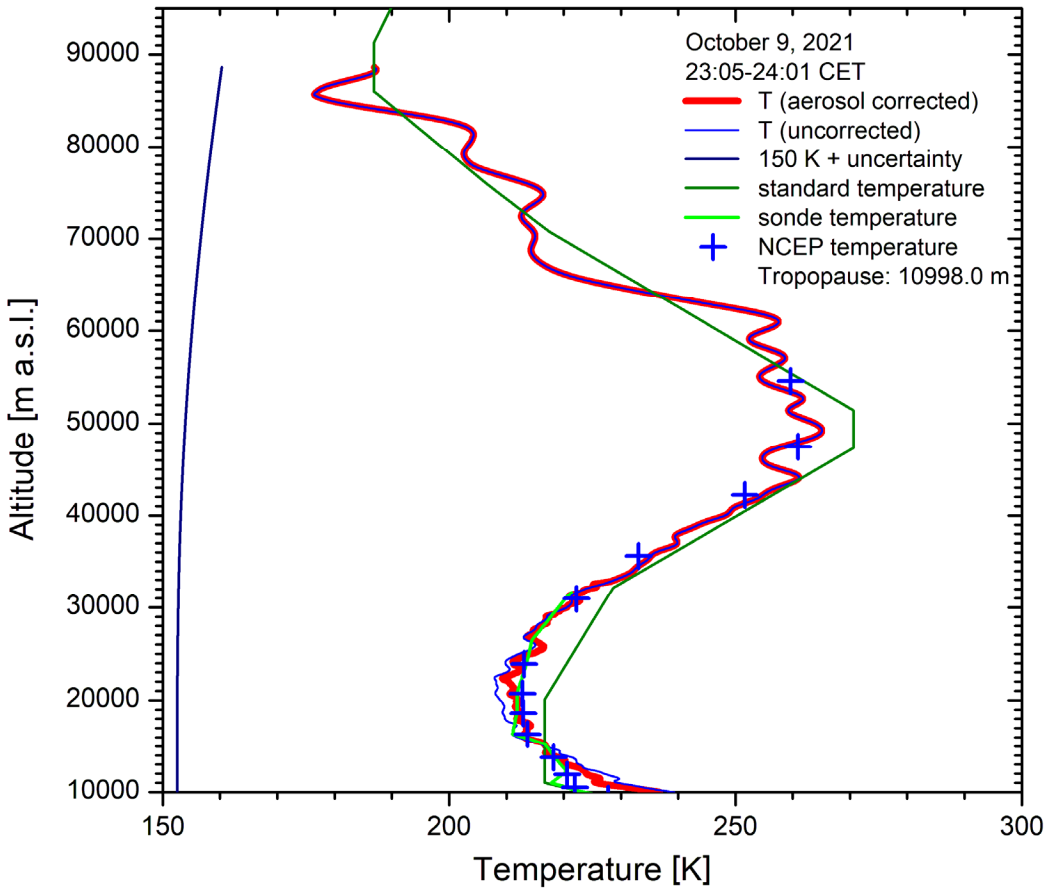

Fig. 4: Temperature profiles for October 9, 2021, from a lidar measurement (blue and red lines), data from the Munich radiosonde (green line) and NCEP (blue crosses) and the U.S. Standard Atmosphere (dark green line). The agreement becomes excellent even below 27 km after making an aerosol correction based on a night-time aerosol measurement. The lidar temperature is highly realistic up to at least 70 km, apart from possibly insufficient smoothing between 43 km and 63 km.

In aerosol retrievals often the scattering ratio

$$R = \frac{\beta_R + \beta_P}{\beta_R}$$

is computed (R: Rayleigh; P: particles). Here, one must be aware that R scales as the reciprocal air number density and considerably amplifies any deviation with growing altitude in the stratosphere. Under background conditions of the stratospheric aerosol ($R \approx 1$) achieving relative uncertainties of less than 5 % above 30 km requires great care.

Finally, for calculating the number density in the lower troposphere corrections of the ideal gas law and to humidity must be taken into account [11,12]. However, these effect are below 1 % and are not further discussed here.

Conclusions

Atmospheric Rayleigh scattering can be calculated with very high accuracy from the existing parameters and the air density obtained from radiosonde ascents or other sufficiently accurate sources. The total Rayleigh extinction cross sections can be synthesized to within 1 % for wavelength above 200 nm and very likely within 0.5 % for wavelengths above 500 nm. Care must be taken for backward scattering which must be calculated based on Eq. 8. This means a correction of about 1.5 % with respect to assuming $F_K(\pi) = F_K$ as most commonly done The Raman spectrum can be calibrated by applying Eqs. 12 and 13 to the sums of Q-branch and all S-branch lines. In any case, more accurate direct measurements of the Rayleigh cross sections are desirable.

The most important source of uncertainty has been that of the radiosonde and satellite-based data used for determining the air number density. However, for radiosounding stations operating the RS92 sonde night-time measurements the results get close to the accuracy requirements for demanding lidar applications. Then potential of nitrogen Raman channels, calibrated a low altitudes, needs to be explored

References

[1] C.-Y. She, Spectral structure of laser light scattering revisited: bandwidth of nonresonant scattering lidars, Appl. Opt **40** (2001), 4875-4884

[2] W. L. Eberhard, Correct equations and common approximations for calculating Rayleigh scatter in pure gases and mixtures and evaluation of differences, Appl. Opt. **49** (2010), 1116-1130

[3] N. J. Bridge, A. D. Buckingham, The polarization of laser light scattered by gases, Proc. Royal Soc. A **295** (1966), 334-349

[4] P. Baierl, W. Kiefer, Theory for Continuum Resonance Raman Scattering in Diatomics using Irreducible Spherical Tensors, J. Raman. Spectrosc. **10** (1981), 197-204

[5] P. Baierl, W. Kiefer, Theory of Depolarization Ratios in Diatomic Molecules for Continuum Resonance Raman Scattering and Applications to $^{79}Br_2$, J. Raman. Spectrosc. **15** (1984), 360-365

[6] R. D. Sharma, Contribution of the polarizability anisotropy to Rayleigh scattering, J. Geophys. Res. **112** (2007), A05306, doi: 10.1029/2006JA011705, 7 pp.

[7] B. Witschas, Analytical model for Rayleigh-Brillouin line shapes in air, Appl. Opt. **50** (2011), 267-270: erratum: Appl. Opt. **50** (2011), 5758

[8] A. T. Young, Rayleigh scattering, Phys. Today, **35 (1)** (1982), 42-48

[9] U. Wandinger, Raman Lidar, pp. 241-271 in: C. Weitkamp, Ed. (Springer, Berlin Heidelberg New York, 2004), Fig. 9.2

[10] R. M. Goody, Extinction by Molecules and Droplets, Sec. 7 (pp. 286-318) in: Atmospheric Radiation, Vol. 1, Theoretical Basis, Oxford at the Clarendon Press (Oxford, U.K., 1964)

[11] J. C. Owens, Optical refractive index of air: dependence on pressure, temperature and composition, Appl. Opt. **6** (1967), 51-59

[12] P. E. Ciddor, Refractive index of air: new equations for the visible and near infrared, Appl. Opt. **35** (1996), 1566-1573

[13] U. Kempfer, W. Carnuth, R. Lotz, T. Trickl, A wide-range UV lidar system for tropospheric ozone measurements: Development and application, Rev. Sci. Instrum. **65** (1994), 3145-3164

[14] E. Hecht, A. Zajac, p. 41 in: Optics, Addison-Wesley (Reading, Massachusetts, 1974), 565 pp.

[15] U.S. Standard Atmosphere 1976, National Oceanic and Atmospheric Administration, NOAA-S/T 76/1562, National Aeronautics and Space Administration, NASA-TM-X 74335, and U.S. Air Force, U.S. Government Printing Office (1976), 241 pp.

[16] E. R. Peck, B. N. Khanna, Dispersion of nitrogen, J. Opt. Soc. Am. **56** (1966), 1059-1063

[17] E. R. Peck, K. Reeder, Dispersion of Air, J. Opt. Soc. Am. **62** (1972), 958-962

[18] R. B. Miles, W. R. Lempert, J. N. Forkey, Laser Rayleigh scattering Meas. Sci. Technol. **12** (2001), R33-R51

[19] D. R. Bates, Rayleigh Scattering by Air, Planet. Space Sci. **32** (1984), 785-790

[20] H. Naus, W. Ubachs, Experimental verification of Rayleigh scattering cross sections, Opt. Lett. **25** (2000), 347-349

[21] M. Sneep, W. Ubachs, Direct measurement of the Rayleigh scattering cross section in various gases, J. Quant. Spectrosc. Radiat. Transfer **92** (2004), 293-310

[22] D. Ityaksov, H. Linnartz, W. Ubachs, Deep-UV Rayleigh scattering of N_2, CH_4 and SF_6, Mol. Phys. **106** (2008), 2471-2479

[23] G. W. Kattawar, A. T. Young, T. J. Humphreys, Inelastic Scattering in Planetary Atmospheres. I. The Ring Effect, Astrophys. J. **243** (1981), 1049-1057.

[24] T. Trickl, H. Giehl, F. Neidl, M. Perfahl, H. Vogelmann, Three decades of tropospheric ozone-lidar development at Garmisch-Partenkirchen, Germany, Atmos. Meas. Tech. **13** (2020), 6357-6390

[25] U. Griesmann, J. H. Burnett, Refractivity of nitrogen gas in the vacuum ultraviolet, Opt. Lett. **24** (1999), 1699-1701

[26] T. Trickl, D. Proch, K. L. Kompa, Resonance-Enhanced 2 + 2 Photon Ionization of Nitrogen: The Lyman-Birge-Hopfield Band System, J. Mol. Spectrosc. **162** (1993), 184-229

[27] T. Trickl, D. Proch, K. L. Kompa, The Lyman-Birge-Hopfield System of Nitrogen: Revised Calculation of the Energy Levels, J. Mol. Spectrosc. **171** (1995), 374-384

[28] G. Rouillé, G. Millot, R. Saint-Loup, H. Berger, High-Resolution Stimulated Raman Spectroscopy of O_2, J. Mol. Spectrosc. **154** (1992), 372-382

[29] G. Y. Golubiatnikov, A. F. Krupnov, Molecular constants of the ground state of oxygen ($^{16}O_2$) accounting for new experimental data, J. Mol. Spectrosc. **225** (2004), 222-224

[30] G. Placzek, E. Teller, Die Rotationsstruktur der Raman-Banden mehratomiger Moleküle, Z. Phys. **81** (1933), 209-258

[31] A. C. Kummel, G. O. Sitz, R. N. Zare, Determination of population and alignment of the ground state using two-photon nonresonant excitation, J. Chem. Phys. **85** (1986), 6874-6897

[32] H. Herzberg, Molecular Spectra and Molecular Structure, I. Spectra of Diatomic Molecules, van Nostrand Reinhold (New York, 1950)

[33] R. L. Rowell, G. M. Aval, J. J. Barrett, Rayleigh-Raman Depolarization of Laser Light Scattered by Gases, J. Chem. Phys. **54** (1971), 1964

[34] A. Young, On the Rayleigh-Scattering Optical Depth of the Atmosphere, J. Appl. Meteor. **20** (1981), 328-331

[35] W. Holzer, Y. Le Duff, K. Altmann, J Dependence of the depolarization ratio of the rotational components of the Q branch of the H_2 and D_2 Raman band, J. Chem. Phys. **58** (1973), 642-643

[36] Y. Yu, K. Lin, X. Zhou, H. Wang, S. Liu, X. Ma, Precise measurement of the depolarization ratio from photoacoustic Raman spectroscopy, J. Raman Spectrosc. **38** (2007), 1206-121

[37] E. W. Eloranta, P. K. Piironen, Adaptation 0d the University of Wisconsin High Spectral Resolution Lidar for Polarization and Multiple Scattering Measurements, 16th International Laser Radar Conference, Cambridge, Massachusetts, July 20-24, 1992, NASA Conference Publications 3158, 4 pp., 1992

[38] V. G. Cooper, A. D. May, E. H. Hara, H. F. P. Knaap, B11-Depolarized Rayleigh Scattering in Gases as a New Probe of intermolecular forces, I.E.E.E. J. Quantum Electron. **4** (1968), 720-722

[39] W. Steinbrecht, H. Claude, F. Schönenborn, U. Leiterer, H. Dier, E. Lanzinger, Pressure and Temperature Differences between Vaisala RS80 and RS92 Radiosonde Systems, J. Atmos. Oceanic Technol. **25** (2008), 909-927

[40] L. Klanner, K. Höveler, D. Khordakova, M. Perfahl, C. Rolf, T. Trickl, H. Vogelmann, A powerful lidar system capable of one-hour measurements of water vapour in the troposphere and the lower stratosphere as well as the temperature in the upper stratosphere and mesosphere, Atmos. Meas. Tech. **14** (2021), 531-555

[41] H. Jäger, Long-term record of lidar observations of the stratospheric aerosol layer at Garmisch-Partenkirchen, J. Geophys. Res. **110** (2005), 9 pp. D08106, doi:10.1029/2004JD005506

[42] T. Trickl, H. Vogelmann, M. D. Fromm, H. Jäger, M. Perfahl, A new generation of the stratospheric aerosol lidar at Garmisch-Partenkirchen – 50 years of lidar vertical sounding, submitted to Atmos. Chem. Phys. for final decision (2023)

[43] L. Klanner, K. Höveler, D. Khordakova, M. Perfahl, C. Rolf, T. Trickl, H. Vogelmann, A powerful lidar system capable of one-hour measurements of water vapour in the troposphere and the lower stratosphere as well as the temperature in the upper stratosphere and mesosphere, Atmos. Meas. Tech. **14** (2021), 531-555